The Astronomical Journal, 165:45 (12pp), 2023 February https://doi.org/10.3847/1538-3881/aca666

Unresolved Binaries and Multiples in the Intermediate Mass Range in Open Clusters: Pleiades, Alpha Per, Praesepe, and NGC 1039

Alina A. Malofeeva[1], Varvara O. Mikhnevich[1], Giovanni Carraro[2], and Anton F. Seleznev[1]
[1] Ural Federal University 19 Mira Street, 620002 Ekaterinburg, Russia
[2] Dipartimento di Fisica e Astronomia, Universita'di Padova Vicolo Osservatorio 3, I-35122, Padova, Italy; giovanni.carraro@unipd.it
Received 2022 September 21; revised 2022 November 22; accepted 2022 November 22; published 2023 January 10

Abstract

In this study, we continue our project to search for unresolved binary and multiple systems in open clusters exploiting the photometric diagram (H–W2)–W1 versus W2–(BP–K) first introduced in Malofeeva et al. In particular, here we estimate the binary and multiple star ratios and the distribution of the component mass ratio q in the Galactic clusters Alpha Persei, Praesepe, and NGC 1039. We have modified the procedure outlined in our first study making star counts automatic and by introducing bootstrapping for error estimation. Basing on this, we reinvestigated the Pleiades star cluster in the same mass range as in our previous work and corrected an inaccuracy in the mass ratio q distribution. The binary and multiple star ratio in the four clusters is then found to lie between 0.45 ± 0.03 and 0.73 ± 0.03. On the other hand, the ratio of systems with multiplicity more than 2 is between 0.06 ± 0.01 and 0.09 ± 0.02. The distribution of the component mass ratio q is well fitted with a Gaussian having the mode between 0.22 ± 0.04 and 0.52 ± 0.01 and the dispersion between 0.10 ± 0.02 and 0.35 ± 0.07. All clusters show a large number of the very low-mass secondary components in the binary systems with primary components below 0.5 $M_{\odot}$.

Unified Astronomy Thesaurus concepts: Open star clusters (1160); Binary stars (154); Multiple stars (1081)

Supporting material: data behind figures

1. Introduction

The first evidence that open star clusters must contain a significant number of unresolved binary systems came out as early as the first half of the past century (Haffner & Heckmann 1937). Since then, a large number of studies have been carried out that demonstrated that the fraction of unresolved binary stars in open clusters usually exceeds 30% (Bonifazi et al. 1990; Khalaj & Baumgardt 2013; Sarro et al. 2014; Sheikhi et al. 2016; Li et al. 2017). A comprehensive review of the topic is given in Duchene & Kraus (2013).

As for the fraction of binary systems, it is widely believed that it increases at increasing the mass of the primary component. Opposite situations, however, have been reported: Patience et al. (2002) for instance found an increase of the fraction of binaries toward lower masses (hence redder colors) in the Alpha Persei and Praesepe clusters.

In the literature various expressions can be encountered for the distribution of the mass ratio of the components of binary systems $q = M_2/M_1$, where M_1 is the mass of the primary component and M_2 is the secondary. Most researchers use a flat distribution (all ratios have the same probability). There are, however, contrasting opinions on whether the q distribution has a maximum near $q = 1$. Duquennoy & Mayor (1991) in fact report that there is no such maximum, whereas Fisher et al. (2005) and Maxted et al. (2008) claim that such a maximum exists both for field stars and for stars in young star clusters. Also Raghavan et al. (2010) support this point of view. Along the same vein, El-Badry et al. (2019) presented strong evidence on the sharp peak at $q = 1$ for field stars at the base of Gaia data. Reggiani & Meyer (2013; for field stars) and Kouwenhoven et al. (2009; for field stars and clusters) first proposed a power law for the q distribution. Kouwenhoven et al. (2009) also suggested a Gaussian distribution for q. Finally, according to Patience et al. (2002), the q distribution is different for different mass intervals.

Thus, the currently available data on the properties of the population of unresolved binary stars in clusters are clearly incomplete and lead to contradictory results.

It should also be noted that data on the q distribution are usually obtained for sufficiently large values of this ratio, since the position of unresolved binary stars with small q on widely used photometric diagrams in the visible wavelengths differs very little from the position of single stars.

The identification and classification of unresolved binary systems in star clusters based on multicolor stellar photometry have been the subject of a number of relatively recent papers. Malkov et al. (2010) exploit the Gaia photometric system and suggest using photometric bands in the ultraviolet range to search for unresolved binary systems (Malkov et al. 2011), but, unfortunately, there are currently no available deep enough photometric data sets in the ultraviolet range. Bardalez Gagliuffi et al. (2014) have proposed methods to identify the unresolved binaries among the very low-mass stars and brown dwarfs using spectroscopic observations. (Geißler et al. 2011) used the cross-comparison of data from the Sloan Digital Sky Survey and Two Micron All Sky Survey (2MASS) surveys for this goal. Unfortunately, the use of only *JHK* filters from the 2MASS survey is insufficient for the reliable detection of unresolved binaries with a small q value.

Borodina & Kovaleva (2020) proposed an original method for studying the population of unresolved binary stars based on Gaia photometry, but, again, the use of photometry only in the visible domain does not allow one to detect unresolved binaries

with a small q value. Finally, Thompson et al. (2021) suggested determining the masses of the components of unresolved binary systems with the main-sequence components in the open clusters by comparing the observed magnitudes in different photometric bands (including ones in the infrared range) with synthetic spectral energy distributions of stars. Nevertheless, multifilter pseudocolor photometric diagrams, in our opinion, allows one to search for unresolved binary systems more effectively and from this to obtain the characteristics of the distribution of binary stars in clusters.

In fact, in our previous study (Malofeeva et al. 2022), we introduced a novel method to evaluate the fraction of unresolved binary stars and higher-multiplicity systems that exploits the pseudocolor diagram (H–W2)–W1 versus W2–(BP–K). This pseudocolor diagram allows us to investigate the population of binaries and multiples in the relatively narrow primary component mass range around the solar mass. This is because for higher masses, single stars and multiple systems do not separate in this diagram. Besides, for a lower mass range the theoretical isochrones of Bressan et al. (2012) do not reproduce the cluster main sequence satisfactorily.

The Pleiades star cluster was used in Malofeeva et al. (2022) as a test bench of the method. We investigated the Pleiades star cluster in the primary component mass range between 0.5 and 1.8 $M_{\odot}$. The binary star ratio was found to lie between 0.54 ± 0.11 and 0.70 ± 0.14. The ratio of systems with a multiplicity larger than 2 was found to be between 0.10 ± 0.00 and 0.14 ± 0.01. The distribution of the component mass ratio q was fitted by a power law with the exponent between -0.53 ± 0.10 and -0.63 ± 0.22. Finally, Malofeeva et al. (2022) stressed that below 0.5 $M_{\odot}$ a large number of brown dwarfs among secondary components is expected in the Pleiades.

However, we realized afterward that the fitting of the q distribution for Pleiades by a power law in Malofeeva et al. (2022) could be significantly improved. In fact, in that analysis, data on the numbers of stars were distributed using variable width q data, and the difference in the bin size was not taken into account explicitly. Therefore, we decided to revisit the fitting of the Pleiades data set using a more robust approach.

First of all, in the present study we use automatic star counts for the various q bins. Second, we apply a bootstrapping method to evaluate the uncertainty of star numbers in the different q bins. And, finally, we model the distribution of the triple and quadruple systems in the (H–W2)–W1 versus W2–(BP–K) diagram in order to better constrain the region occupied by them and having the primary component in the desired mass range.

As a consequence, the layout of the paper is as follows. Section 2 is devoted to the revision of the Pleiades results. In Section 3 we describe the new findings for the Alpha Persei and Praesepe star clusters. Section 4, then, is dedicated to the investigation of the star cluster NGC 1039. Finally, Section 5 summarizes our results.

2. A New Look at the Pleiades Star Cluster

Following Malofeeva et al. (2022), we used the diagram (H–W2)–W1 versus W2–(BP–K) to search for unresolved binary and multiple stars among the Pleiades probable cluster members. We remind the reader that the sample was constructed as the intersection of two data sets. The first one comes from Danilov & Seleznev (2020) and it includes stars inside a circle of $10\overset{\circ}{.}9$ wide up to $G = 18$ mag. The probability of being a cluster member is 95% or higher, and the completeness is around 90%. The second source comes from Lodieu et al. (2019), and from this we took the photometric data.

Figure 1 shows the diagram for the selected stars with superimposed theoretical lines of constant q values. The rightmost line corresponds to $q = 0$, i.e., the single-star sequence. The leftmost line corresponds to $q = 1$, and it is the equal component mass binary sequence. We plotted these theoretical lines using isochrone tables from Bressan et al. (2012) and following the procedure described in Malofeeva et al. (2022). The cluster parameters $\log t = 8.116$, metallicity $[\mathrm{M/H}] = 0.032$, extinction $A_V = 0.168$, and the distance to the cluster of 135 pc are extracted from Dias et al. (2021).

A quick glance at Figure 1 shows that the lines of constant q values overlap in the upper part of the diagram. On the other hand, in the lower part of the diagram the lines of constant q values do not coincide well with the cluster sequence, as already stressed in Malofeeva et al. (2022). Finally, one can notice that the various isolines terminate sharply in the lower part of the diagram due to the lack of data on stars with masses lower than 0.1 $M_{\odot}$ in the isochrone tables of Bressan et al. (2012).

Therefore, when counting stars in this diagram of Figure 1, we are limited by the mass of the primary component in the range from 0.5 to 1.8 $M_{\odot}$.

We introduced some improvements with respect to the original procedure developed in Malofeeva et al. (2022). First, we determined more accurately the upper and lower boundaries of the region of stars with a multiplicity greater than 2 (dashed lines in Figure 2 leftward of the $q = 1$ line). To achieve this, we have modeled 600 triple and 600 quadruple star systems with the masses of the primary component from 0.5 to 1.8 $M_{\odot}$, and the masses of other components from 0.1 $M_{\odot}$ up to the mass of the main component. The masses of the primary components were distributed as a geometrical progression (with the use of the numpy.geomspace routine). This distribution is close to a uniform one in log space, but all the mass values are unique (not repeated), and the number of low-mass stars is larger than in the uniform case. Note that the main goal in this case is to show in the best possible way how binary and higher-multiplicity systems are distributed. Realistic mass distributions are ill suited for this, since they give a much smaller number of massive stars compared to low-mass ones. The goal of this choice is to achieve a better representation of the region occupied by the triple and quadruple systems with the primary component mass in the range of interest. Figure 2 shows the location of the unresolved triple and quadruple stars in the diagram. The blue and orange lines correspond to triple and quadruple unresolved systems with equal components. The thin black lines are lines of equal q values in the order described in the capture to Figure 2. It can be noticed that the regions of triple and quadruple systems overlap with the region of binary stars. Therefore, some of the Pleiades stars identified as binary may actually turn out to be triple or quadruple stars. As a consequence, the estimate of the binary star number would be an upper one. In turn, the estimates of the number of triple and quadruple stars would be the lower ones, if we count stars between the left thin black line and the blue line for triple stars, and between the blue line and the orange line for quadruple stars.

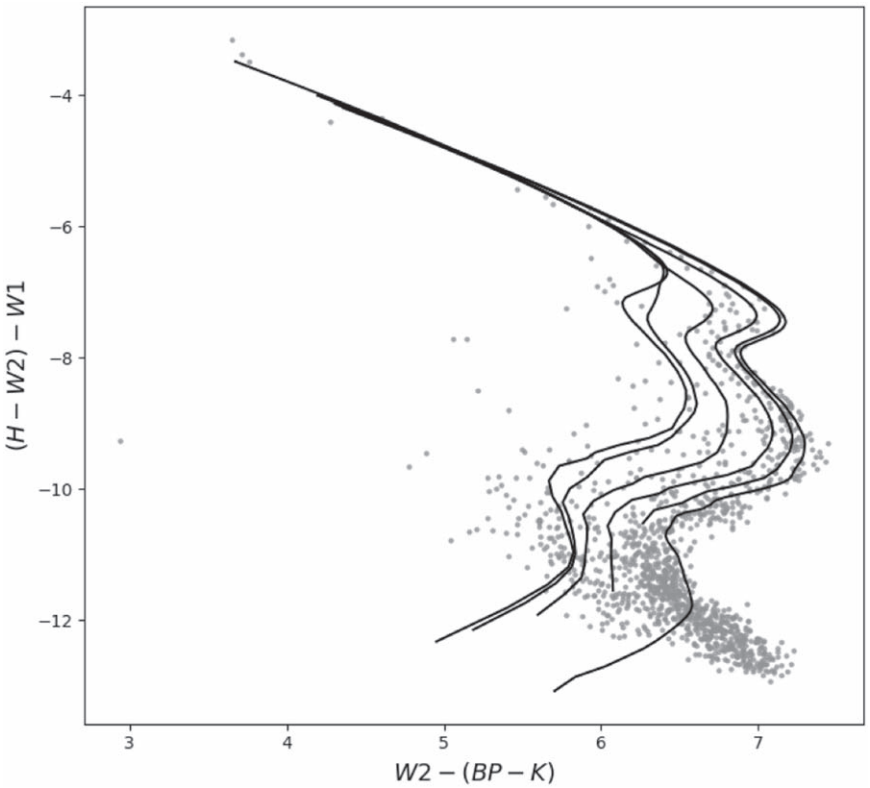

Figure 1. W2–(BP–K) vs. (H–W2)–W1 diagram for the sample of the Pleiades probable members. Solid lines are for constant q values. These lines of constant q values refer to the Bressan et al. (2012) isochrone with $\log t = 8.116$. q values are 0.0, 0.2, 0.4, 0.6, 0.8, and 1.0 (from the right to the left).

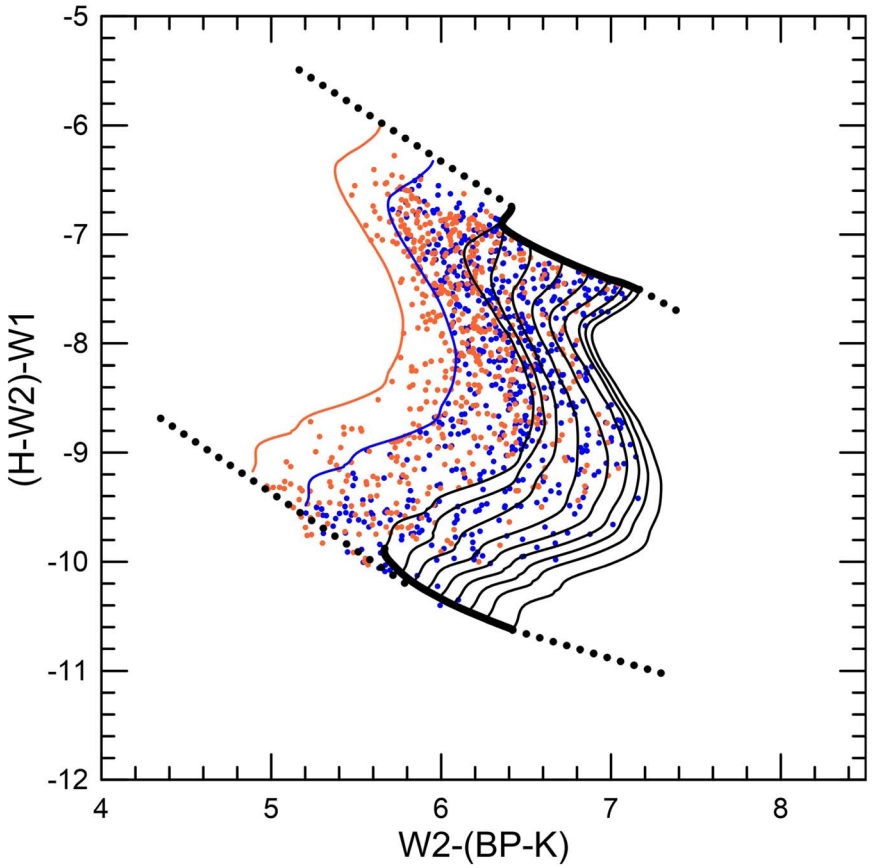

Figure 2. (H–W2)–W1 vs. W2–(BP–K) diagram for triple and quadruple unresolved stars with the primary component in the range between 0.5 and 1.8 $M_{\odot}$. Blue dots are triple stars. Orange dots are quadruple stars. The blue and orange lines correspond to triple and quadruple unresolved systems with equal components. The thin black lines are lines of equal q values in the following order (from the right to the left): $q = 0$, 0.2, 0.3, 0.4, 0.5, 0.6, 0.7, 0.8, and 1.0.

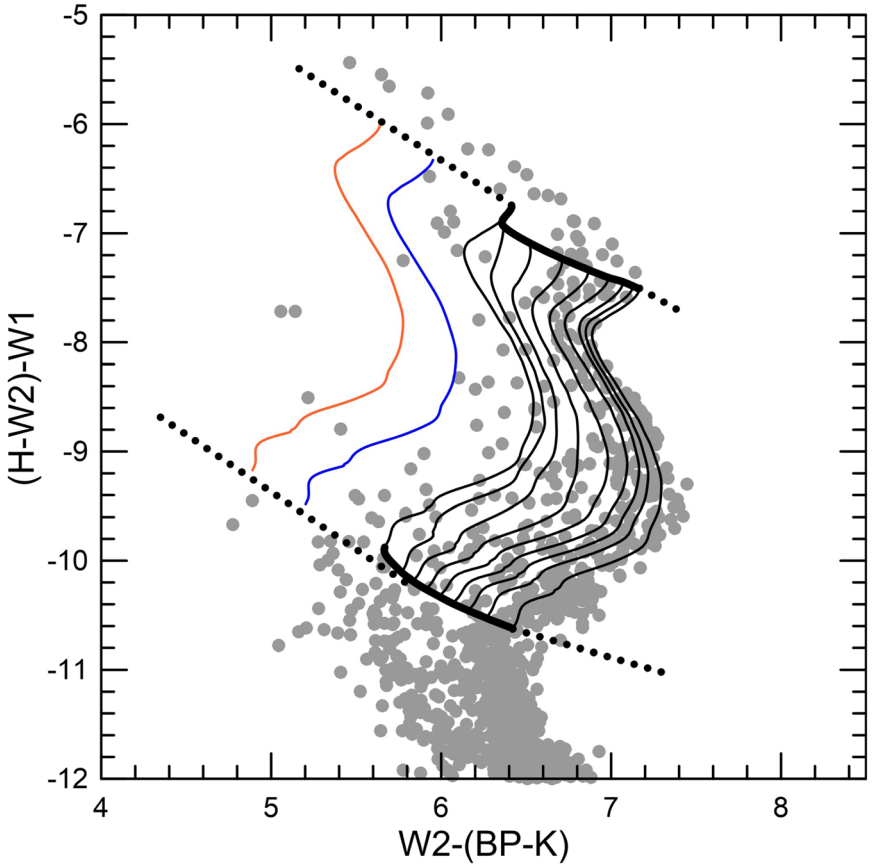

Figure 3. (H–W2)–W1 vs. W2–(BP–K) diagram for Pleiades probable members (gray dots) with superimposed lines of constant q values (as in Figure 2), lines for multiple systems with equal components (as in Figure 2), and with the boundaries (thick solid and dashed lines) of the area of star counts.
(The data used to create this figure are available.)

Figure 3 shows the pseudocolor diagram with the upper and lower boundaries of the star counting area. The upper line corresponds to binary and multiple stars with the primary component of 1.8 $M_{\odot}$. The lower line corresponds to binary and multiple stars with the primary component of 0.5 $M_{\odot}$.

The second improvement is that we have made the bins covering equal intervals in q for a correct construction of the q distribution $f(q)$. It turns out that the $f(q)$ has a maximum at $q \sim 0.3$–0.4 (Figures 4, 7, 8, 10, and Table 3).

The counting of the single stars was performed in the same way as in the previous work (Malofeeva et al. 2022). Since single stars are plotted on the diagram with errors, they fall on both sides of the theoretical line of single stars ($q = 0$). Therefore, we propose to consider them in two ways. In the first case (case (a)), and with reference to Figure 3, only points rightward of the single-star ($q = 0$) sequence are considered to be single stars. In the second case (case (b)), we add points with q from 0 to 0.2 to the single-star sample. The upper and lower boundaries of the region of single stars are drawn as tangents to the lines of binary stars with the primary components with a mass of 0.5 and of 1.8 $M_{\odot}$. Star counts were performed automatically. For every q bin, the position of each star relative to the lines bounding this bin was determined by linear interpolation.

Another important improvement with respect to our previous study (Malofeeva et al. 2022) is the use of a bootstrap method to account for photometric errors. In detail, the observational data points were replotted randomly according to a normal distribution with the mean and standard deviation taken from the catalog for any given star, and the procedure of the star counts repeated. Bootstrapping was repeated 100 times, then the average values of the number of stars in the q bins and their standard deviations were computed. The results of star counts in different q bins are shown in Table 1 for the Pleiades, Alpha Persei, and Praesepe star clusters.

Table 1
The Results of Counts of Stars with Different Values of q in Pleiades, Alpha Per, and Praesepe Clusters

The Range of q	Number of Stars Pleiades	Number of Stars Alpha Per	Number of Stars Praesepe
to the right of $q = 0$	112 ± 5	123 ± 6	89 ± 4
$0 < q < 0.2$	74 ± 6	60 ± 6	35 ± 5
$0.2 < q < 0.4$	81 ± 5	65 ± 5	47 ± 5
$0.4 < q < 0.6$	69 ± 5	54 ± 4	19 ± 2
$0.6 < q < 0.8$	34 ± 3	24 ± 2	15 ± 2
$0.8 < q < 1.0$	10 ± 2	6 ± 2	6 ± 2
triple systems	29 ± 2	20 ± 2	13 ± 2
quadruple systems	3 ± 1	2 ± 1	1 ± 1

Figure 1 indicates also a systematic deviation of the star sequence rightward of the $q = 0$ line, and below $(H - W_2) - W_1 \sim -8.4$ (exactly as in our previous work; Malofeeva et al. 2022). We envisage two possible reasons for

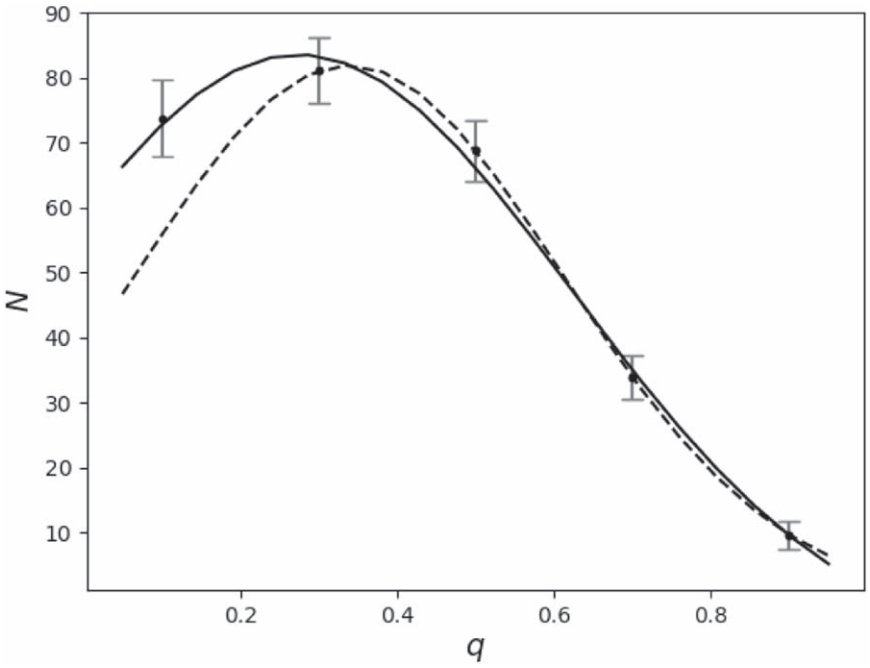

Figure 4. The distribution of the component mass ratio q and its fitting by a Gaussian for the Pleiades. Solid line (case (a))—stars with $0 < q < 0.2$ are considered as binaries; dashed line (case (b))—stars with $0 < q < 0.2$ are added to singles.

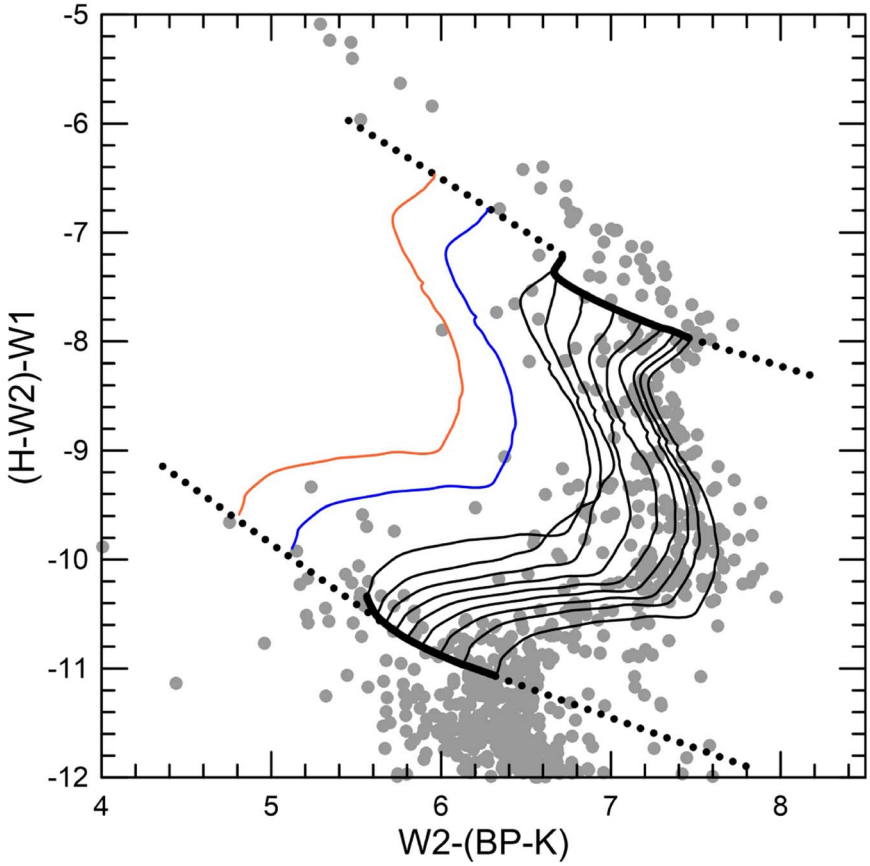

Figure 5. The (H–W2)–W1 vs. W2–(BP–K) diagram for the probable members of the Alpha Persei (gray dots). Lines and designations are the same as in Figure 3. The upper lines correspond to the binary and multiple stars with a primary component of 1.9 $M_{\odot}$. The lower lines correspond to the binary and multiple stars with a primary component of 0.5 $M_{\odot}$.

(The data used to create this figure are available.)

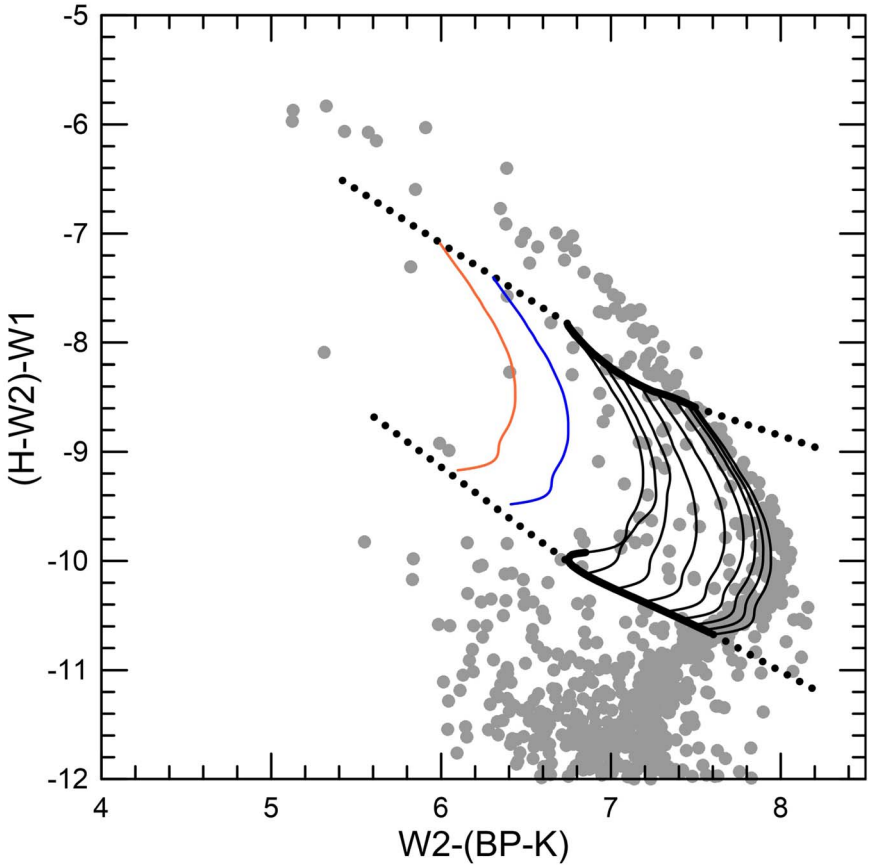

Figure 6. The (H–W2)–W1 vs. W2–(BP–K) diagram for the probable members of the Praesepe (gray dots). Lines and designations are the same as in Figure 3. The upper lines correspond to the binary and multiple stars with a primary component of 1.4 $M_{\odot}$. The lower lines correspond to the binary and multiple stars with a primary component of 0.7 $M_{\odot}$.

(The data used to create this figure are available.)

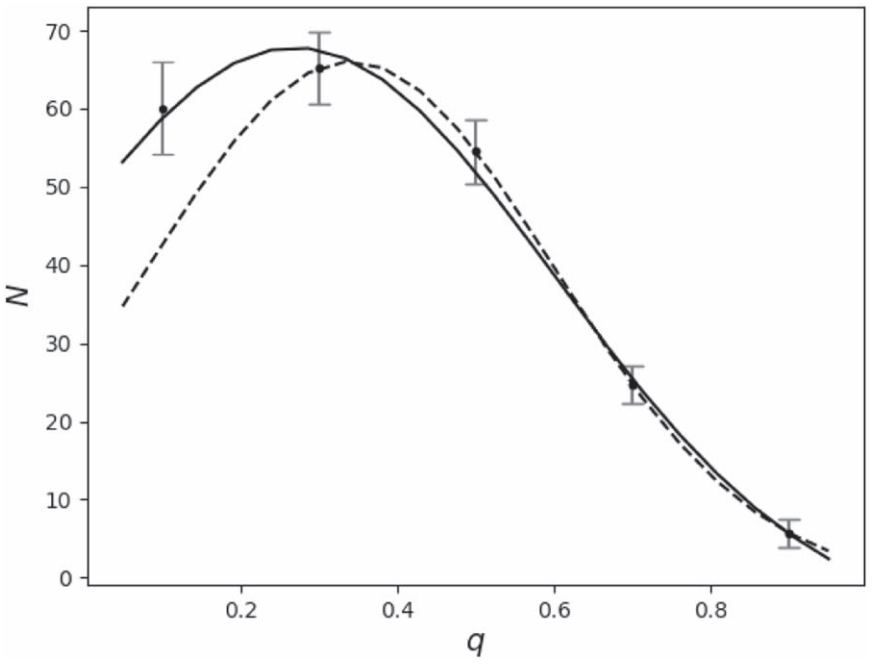

Figure 7. The distribution of the component mass ratio q and the Gaussian fit for the Alpha Persei cluster. Designations are the same as in Figure 4.

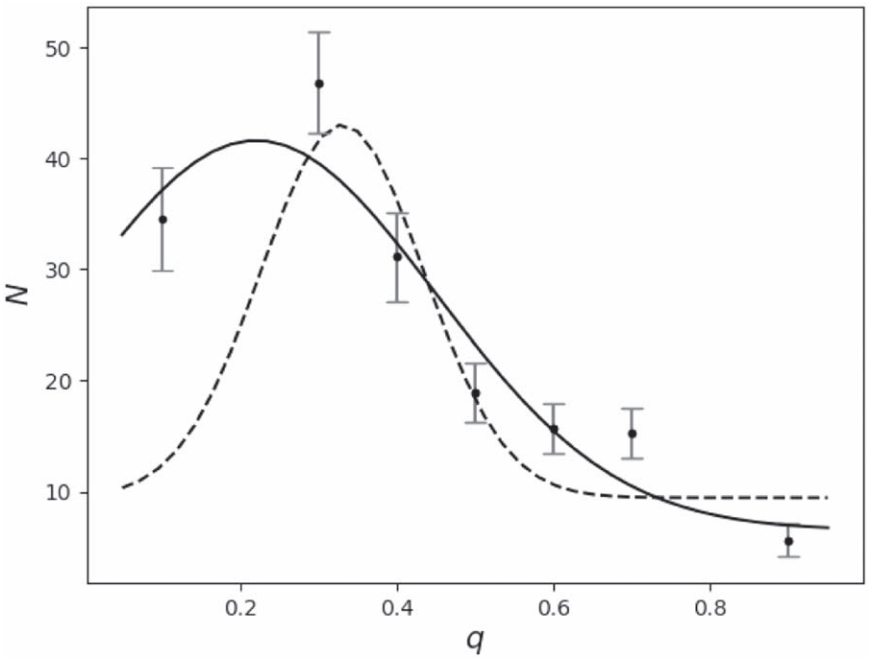

Figure 8. The distribution of the component mass ratio q and the Gaussian fit for the Praesepe cluster. Designations are the same as in Figure 4.

Table 2
The Results of Counts of Stars in the Narrow q Bins in the Praesepe Cluster

The Range of q	Number of Stars Praesepe
$0.2 < q < 0.3$	27 ± 4
$0.3 < q < 0.4$	20 ± 3
$0.4 < q < 0.5$	11 ± 2
$0.5 < q < 0.6$	8 ± 2
$0.6 < q < 0.7$	8 ± 1
$0.7 < q < 0.8$	7 ± 2

this occurrence. First of all this is probably the cumulative effect of increasing the number of stars and the photometric errors (see Figure 3(a) from Malofeeva et al. 2022). Besides, it might also originate from the isochrone fitting procedure, which is effective in the upper part of the diagrams, but exhibits a clear mismatch with the cluster sequence downward of −8.4. We anticipate that this occurs in all the clusters under consideration (Figures 3, 5, 6, 9).

This deviation can artificially increase single-star counts. However, this is partially accounted for by our procedure because the typical values of the pseudocolor errors are comparable with the star count variations.

Figure 4 shows the distribution function $f(q)$ for the first case (single stars are only to the right of the line $q = 0$, the solid line, case (a)) and the second case (stars in the bin $q \in [0; 0.2]$ are added to single stars, the dashed line, case (b)). Since there is a clear maximum around $q \sim 0.3$–0.4, we followed Kouwenhoven et al. (2009) and performed the fitting by a Gaussian function using a nonlinear least-squares method with errors (using the *curve_fit* routine from the Python package scipy.optimize):

$$dN/dq \sim \exp[-(q - \mu_q)^2/2\sigma_q^2]. \quad (1)$$

The mean values and standard deviations were equal to $\mu = 0.27 \pm 0.03$ and $\sigma = 0.35 \pm 0.07$ for case (a) and $\mu = 0.34 \pm 0.06$ and $\sigma = 0.27 \pm 0.07$ for case (b). For the parameters α

$$\alpha = \frac{N_{\rm binaries} + N_{\rm triples} + N_{\rm quadruples}}{N_{\rm singles} + N_{\rm binaries} + N_{\rm triples} + N_{\rm quadruples}}, \quad (2)$$

β

$$\beta = \frac{N_{\rm triples}}{N_{\rm binaries} + N_{\rm triples} + N_{\rm quadruples}}, \quad (3)$$

and γ

$$\gamma = \frac{N_{\rm quadruples}}{N_{\rm binaries} + N_{\rm triples} + N_{\rm quadruples}}, \quad (4)$$

we obtained the values listed in Table 3 along with the parameters of the q distribution (Table 3; Sections 3 and 4). This result is in line with our previous study (Malofeeva et al. 2022).

The conclusion of Malofeeva et al. (2022) on the presence of a large number of the binary systems with very low-mass secondary components (quite probably, brown dwarfs) in the Pleiades remains unaltered. We discuss this point in more details below.

3. Binary and Multiple Star Populations in Alpha Per and Praesepe Star Clusters

We obtained the parameters of the populations of binary and multiple stars in the Alpha Persei and Praesepe clusters in the same way as in the Pleiades, exploiting the photometric diagram of (H–W2)–W1 vs. W2–(BP–K). For the Alpha Persei cluster, we used an isochrone with $\log t = 7.921$, metallicity $[M/H] = 0.158$, extinction $A_V = 0.324$, and the distance to the cluster $r = 177$ pc. For the Praesepe cluster, we used an isochrone with $\log t = 8.882$, metallicity $[M/H] = 0.196$, extinction $A_V = 0.032$, and the distance to the cluster $r = 186$ pc. These sets of cluster parameters were extracted from Dias et al. (2021).

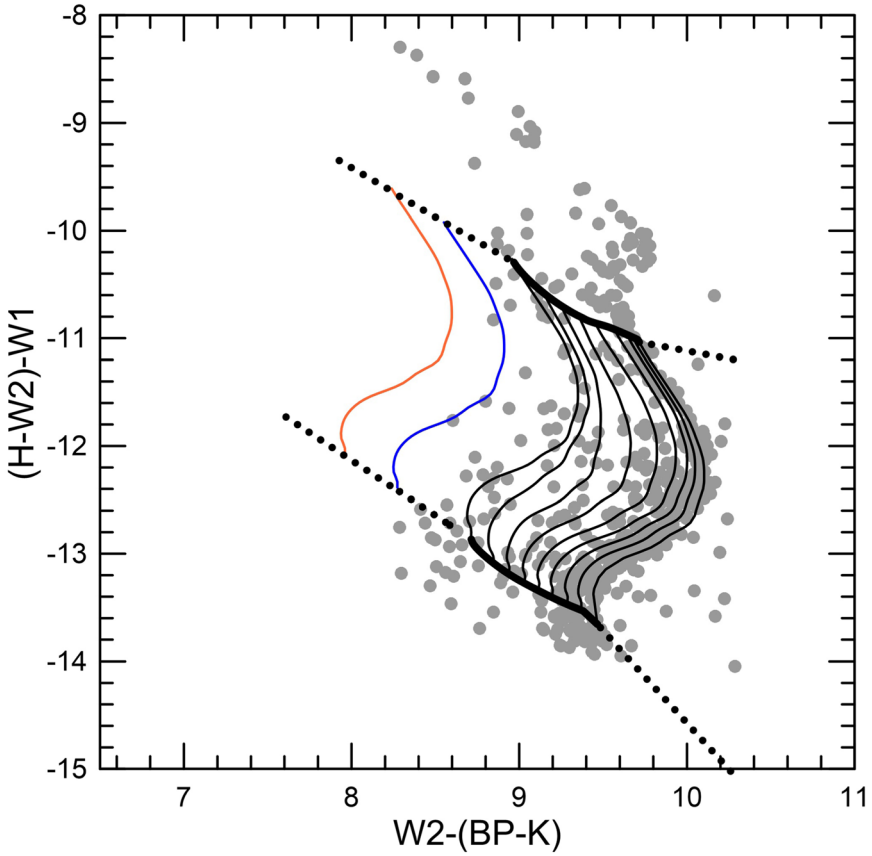

Figure 9. The diagram (H–W2)–W1 vs. W2–(BP–K) for the probable members of NGC 1039 (gray dots) with the thin black lines for constant q values of 0.0, 0.2, 0.3, 0.4, 0.5, 0.6, 0.7, 0.8, and 1.0 (from the right to left), and with the boundaries of the area of star counts. An upper line corresponds to binary and multiple stars with the primary component of 1.3 $M_{\odot}$. A lower line corresponds to binary and multiple stars with the primary component of 0.5 $M_{\odot}$. The blue and orange lines designate triple and quadruple systems with equal components, respectively.

(The data used to create this figure are available.)

Table 3
Parameters of the Binary and Multiple Star Population in the Clusters

Parameter	Pleiades	Alpha Persei	Praesepe	NGC 1039
μ (Case (a))	0.27 ± 0.03	0.27 ± 0.03	0.22 ± 0.04	0.51 ± 0.02
μ (Case (b))	0.34 ± 0.06	0.34 ± 0.05	0.33 ± 0.02	0.52 ± 0.01
σ (Case (a))	0.35 ± 0.07	0.32 ± 0.05	0.23 ± 0.04	0.23 ± 0.02
σ (Case (b))	0.27 ± 0.07	0.25 ± 0.05	0.10 ± 0.02	0.20 ± 0.01
α (Case (a))	0.73 ± 0.03	0.65 ± 0.03	0.60 ± 0.04	0.70 ± 0.02
α (Case (b))	0.55 ± 0.02	0.48 ± 0.02	0.45 ± 0.03	0.63 ± 0.02
β (Case (a))	0.10 ± 0.01	0.09 ± 0.01	0.10 ± 0.02	0.11 ± 0.02
β (Case (b))	0.13 ± 0.01	0.12 ± 0.01	0.13 ± 0.02	0.13 ± 0.02
γ (Case (a))	0.010 ± 0.003	0.009 ± 0.004	0.007 ± 0.007	0.02 ± 0.01
γ (Case (b))	0.013 ± 0.004	0.012 ± 0.006	0.010 ± 0.010	0.02 ± 0.01

Samples of probable cluster members of the Alpha Persei and Praesepe clusters were built from the catalog of Lodieu et al. (2019). We excluded stars with $G > 18$ mag. Some stars below the cluster main sequence on the color–magnitude diagram (CMD) also were excluded. The sample of the probable cluster members of the Alpha Persei cluster is the intersection of the Lodieu et al. (2019) sample and the cluster sample *C2*, obtained in Nikiforova et al. (2020) with DBSCAN to avoid the contamination by stars belonging to the stellar stream in the vicinity of the Alpha Persei cluster. Eventually, the sample of the Alpha Persei probable members contains 956 stars, whereas the sample of the Praesepe probable members contains 2200 stars. The theoretical sequences of single and binary stars, namely the lines of constant q, the upper and lower boundaries of the regions for star counts, and the lines for multiple systems with equal components, were plotted in the same way as for Pleiades. Figures 5 and 6 contain the resulting color–color diagrams with theoretical lines and member stars of the Alpha Persei and the Praesepe cluster, respectively. The lower and upper bounds for Alpha Persei correspond to stars with masses of the main components of 0.5 and 1.9 $M_{\odot}$, while for the Praesepe, of 0.7 and 1.4 $M_{\odot}$.

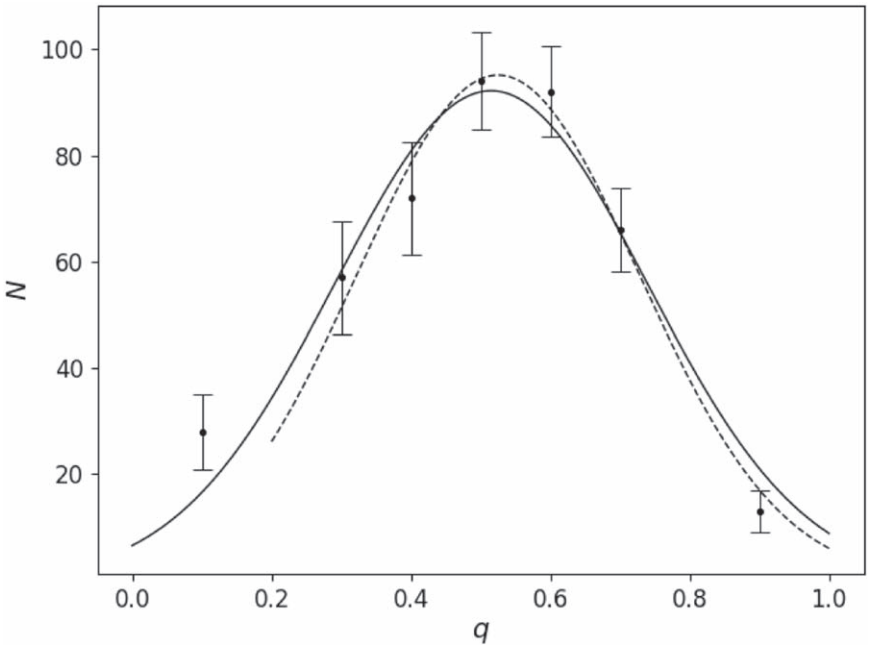

Figure 10. The distribution of the component mass ratio q and its fitting by a Gaussian for NGC 1039. Solid line is for case (a) while dashed line is for case (b).

The procedure of star counts in the q bins and multiple bins, and the accounting of photometry errors for the Alpha Persei and Praesepe clusters were exactly the same as for the Pleiades (see above). The results of star counts are then listed in Table 1. On the other hand, the distribution functions of the q parameter for Alpha Persei is shown in Figure 7. For the Praesepe cluster we faced a problem since excluding the point corresponding to the q bin [0; 0.2] the fitting routine could not return acceptable parameters for the Gaussian curve. To circumvent this problem we performed star counts for Praesepe cluster in narrower q bins (of 0.1 width) to increase the number of points for the fitting. The results of star counts for Praesepe with a narrow bin choice are listed in Table 2. Then, to provide the equal bins of 0.2 for fitting, in line with the other clusters, we used the sum of two adjacent narrower bins.

For Praesepe, moreover, case (b), when we consider stars in the bin $q \in [0; 0.2]$ as single stars, corresponds to assuming that the number of the binary stars in that bin is equal to zero. This way we could solve the problem for the Praesepe cluster (see Figure 8 for the distribution of q and its fitting). Table 3 lists the parameters of the distribution of q (fitted by Gaussian Equation (1)) and the values of α, β, and γ for clusters.

4. Binary and Multiple Star Populations in NGC 1039

We have searched for unresolved binaries and multiple stars in the open star cluster NGC 1039 applying the procedure described above to a sample of probable cluster members. This sample was compiled starting from the catalog of Cantat-Gaudin et al. (2020) with the photometry from Gaia DR2 on the condition $G \leqslant 18$. We have added the necessary photometric bands from the catalogs of 2MASS (Skrutskie et al. 2006) and WISE (Cutri 2012) surveys. We have excluded stars with a membership probability less than 50%. As a result, the final sample contains 553 stars.

We construct the theoretical sequence of single stars and lines of the constant q values using the isochrone tables of Bressan et al. (2012) with the age logarithm $\log t = 8.116$, metallicity $[\mathrm{Fe/H}] = -0.006$, and extinction $A_V = 0.328$. These cluster parameters and the distance to the cluster of $r = 507$ pc were again extracted from Dias et al. (2021). Figure 9 shows the diagram with the theoretical lines, the cluster stars, and the lower and upper limits corresponding to systems with the primary component mass of 0.5 $M_\odot$ and 1.3 $M_\odot$, respectively. As for the case of the Pleiades (Section 2; Figure 2), we have modeled the distribution of the triple and quadruple systems with the primary component mass in the same range in order to better outline the region occupied by multiple systems.

Table 4
Results of Counts of Stars with Different Values of q and Multiple Stars in NGC 1039

The Range of q	Number of Stars NGC 1039
to the right of $q = 0$	109 ± 9
$0 < q < 0.2$	28 ± 8
$0.2 < q < 0.3$	27 ± 7
$0.3 < q < 0.4$	32 ± 8
$0.4 < q < 0.5$	42 ± 8
$0.5 < q < 0.6$	53 ± 6
$0.6 < q < 0.7$	40 ± 6
$0.7 < q < 0.8$	28 ± 6
$0.8 < q < 1.0$	13 ± 4
triple systems	30 ± 6
quadruple systems	5 ± 3

The procedure of counting multiple, binary, and single stars and accounting for photometric errors are the same as described above for the Pleiades, Alpha Persei, and Praesepe. The only difference is that the bootstrapping procedure has been performed 300 times in this case, because we noted that 100 times was insufficient for this cluster to reach stable results. The results of star counts are listed in Table 4, while the distribution functions of the q parameter are shown in Figure 10. In order to keep the q bins equal ($\Delta q = 0.2$) the data from Table 4 were stacked in the following way: $0.2 < q < 0.3$ and $0.3 < q < 0.4$, $0.3 < q < 0.4$ and $0.4 < q < 0.5$,

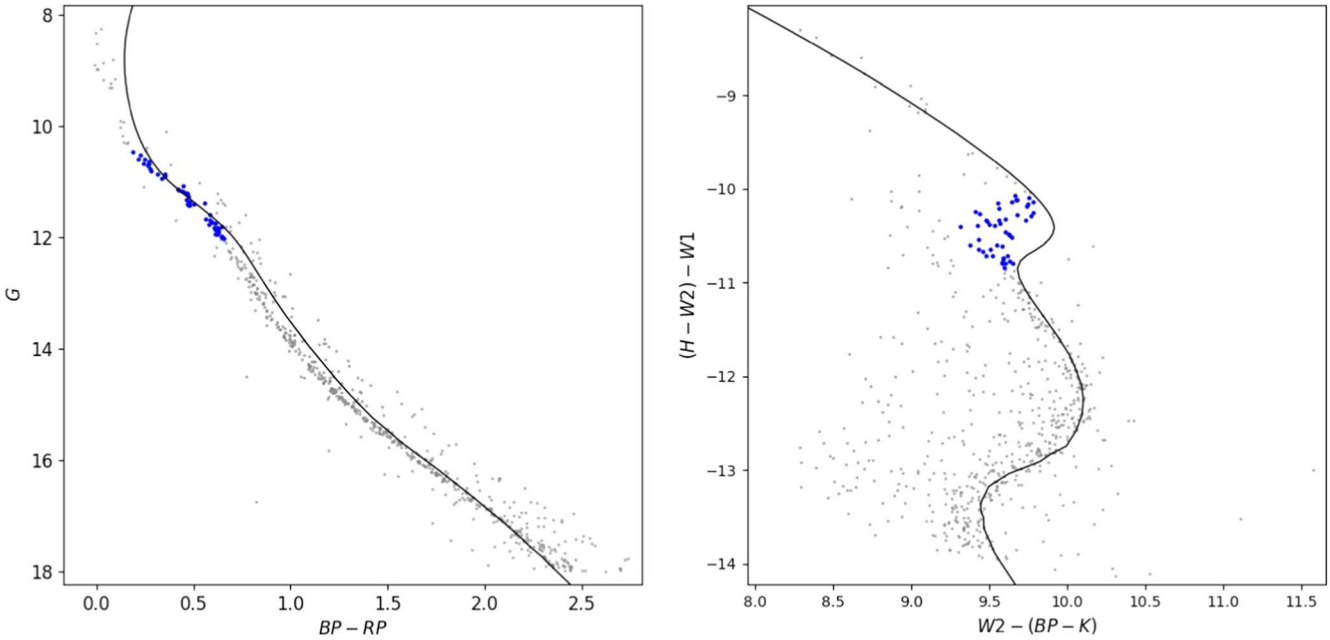

Figure 11. The NGC 1039 CMD (left) and the diagram W2–(BP–K) vs. (H–W2)–W1 (right). The solid line represents the theoretical isochrone overimposed for the set of cluster parameters from Dias et al. (2021). The blue dots mark the same stars on both diagrams.

$0.4 < q < 0.5$ and $0.5 < q < 0.6$ and so on. The distribution of q was fitted with a Gaussian for two cases (including the point for the bin $0.0 < q < 0.2$ and without it). The parameters of the Gaussian and the ratios of the binary and multiple stars are listed in the last column of Table 3.

5. Conclusions

In this study, we investigated the population of binary and multiple stars in the Pleiades, Alpha Persei, Praesepe, and NGC 1039 Galactic star clusters. To this purpose, we used a photometric diagram that employs two pseudocolors constructed from stellar magnitudes in the passbands of visible and infrared wavelengths W2–(BP–K) versus (H–W2)–W1, originally proposed by Malofeeva et al. (2022). The advantage of this color combination is that binary stars in this diagram clearly pop up and are well distinguished from single stars even for small values of the component mass ratio q.

The most important limitation of our investigation is that theoretical isochrones (the line of single stars, $q = 0$) do not coincide well with the cluster main sequence for the whole stellar magnitude range. Because of that, we were forced to limit the range of our exploration of this diagram to intermediate masses for the primary component: $M_1 \in [0.5; 1.8]\ M_\odot$ for Pleiades, $M_1 \in [0.5; 1.9]\ M_\odot$ for Alpha Persei, $M_1 \in [0.7; 1.4]\ M_\odot$ for Praesepe, and $M_1 \in [0.5; 1.3]\ M_\odot$ for NGC 1039.

We used the fundamental cluster parameters from the catalog of Dias et al. (2021). As an illustration, Figure 11 shows the CMD for NGC 1039 (the left panel) and the diagram W2–(BP–K) versus (H–W2)–W1 for this cluster (the right panel). In general the fitting is rather disappointing. If one tries to adjust the upper part of the diagram, the lower part gets off, and vice versa. The blue dots in Figure 11 mark the same stars on both diagrams. It is well visible that while on the CMD these stars are close enough to the isochrone, on the diagram W2–(BP–K) versus (H–W2)–W1 the same stars are far from the isochrone. The reason is unclear, but it is because of this point that we had to limit the mass range of our investigation.

In the case of the Pleiades we improved on Malofeeva et al. (2022) fitting of the q distribution with the implementation of equal q bins. As a result, it turned out that a power law is not suitable because this distribution has a maximum for all clusters under investigation. We used a Gaussian curve instead following Kouwenhoven et al. (2009), with the parameters of the fitting listed in Table 3. The mode of distribution ranges from 0.22 for Praesepe to 0.52 for NGC 1039. The dispersion ranges between 0.10 ± 0.02 for Praesepe and 0.35 ± 0.07 for Pleiades.

The parameters of the q distribution are close to each other except for the mode in NGC 1039 and the dispersion in Praesepe (for the case (b) single-star number estimate; in this case the approximation includes the additional condition of the absence of binaries with $q \in [0; 0.2]$). The ratio of the binary and multiple stars and ratios of the triple and quadruple systems also are close for the sample clusters (Table 3). We could not find any correlation of these parameters with the cluster age.

An important point is the relatively small number of binaries with equal mass components. This seems to contradict the results of El-Badry et al. (2019). A possible explanation for this contradiction is that we take into account the unresolved systems only. Another possibility is that tight resolved binaries with similar components could have bad Gaia astrometric solutions and be missed in the samples of probable cluster members.

All clusters show a large number of very low-mass secondary components in the binary systems with primary components below 0.5 $M_\odot$. We expect that in general these secondary components are brown dwarfs. This point is illustrated in Figure 12 for all four clusters. The general problem is that the theoretical isochrone (line of $q = 0$) and theoretical lines for constant q values do not coincide well with the clusters' sequence, as already stressed. Due to this fact we tried to position by eye the "correct" q lines following the cluster sequence (red lines in Figure 12). In the case of NGC

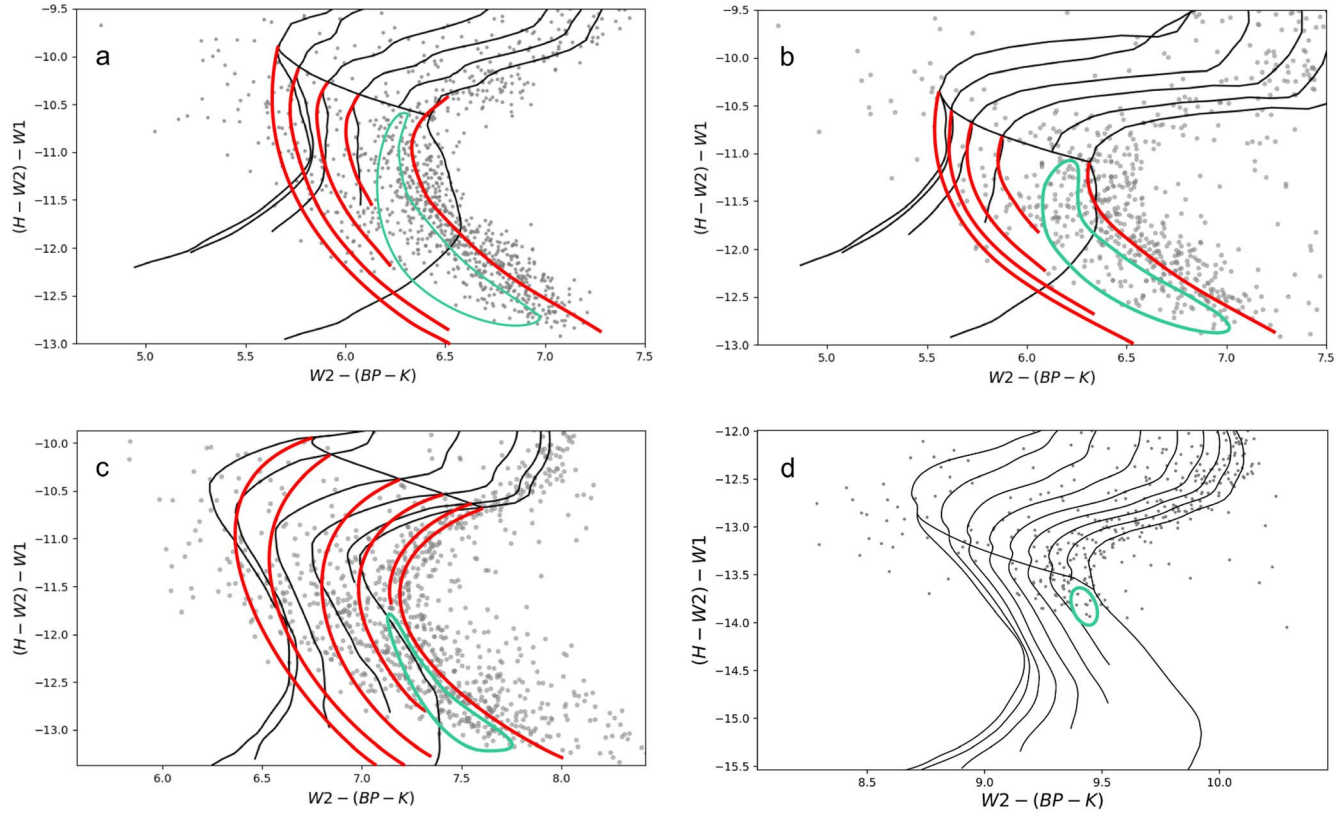

Figure 12. The lower parts of the W2–(BP–K) vs. (H–W2)–W1 diagram for all four clusters. (a) Pleiades. (b) Alpha Persei. (c) Praesepe. (d) NGC 1039. Gray dots indicate cluster stars, while black lines are theoretical lines of constant q values. The red lines are the probable "correct" lines of constant q values plotted by eye following the cluster sequence. The green lines outline the probable region occupied by binary systems with the secondary component of the mass lower than 0.1 $M_{\odot}$.

1039 we could not achieve this because the cluster sequence sharply disappears below the primary component for the 0.5 $M_{\odot}$ line. The green lines in Figure 12 outline the probable region occupied by binary systems with the secondary component mass smaller than 0.1 $M_{\odot}$. They also were positioned by eye.

Clearly, we cannot consider these arguments as strong evidence. Most of all, the difficulties of fitting isochrones to the cluster sequence hamper a more solid and quantitative analysis. Besides, in the case of the faintest stars, we cannot exclude a fraction of random contamination among probable cluster members. In spite of all these limitations, we believe that the presence of the low-mass components in the binary systems and the brown dwarfs among them is quite probable.

In the considered mass range the binary and multiple star ratio is between $\alpha = 0.45 \pm 0.03$ for Praesepe and $\alpha = 0.73 \pm 0.03$ for Pleiades. The ratio of the multiple stars with multiplicity greater than 2 is between 0.06 ± 0.01 for Alpha Persei and Praesepe and 0.09 ± 0.02 for NGC 1039. These estimates are larger than previously found (see a review above and in Malofeeva et al. 2022). We can easily account for this result since our diagram allows one to detect unresolved binaries with smaller component mass ratios that were clearly missed in previous investigations.

We also provide lower estimates for the number of triple and quadruple systems. Figures 3, 5, and 6 show the presence of stars that corresponds to the theoretical location of systems with a multiplicity greater than 4. However, the presence of such systems seems rather unreliable because stable systems with a multiplicity greater than four should be resolved at distances of the Pleiades, Alpha Persei, and Praesepe clusters. On the other side, it seems that the probability of finding stable quintuple or sextuple system in the cluster is very low because such systems should be wide (hierarchic) and easily disrupted by encounters with other stars. The origin of stars in the far left side of the diagram W2–(BP–K) versus (H–W2)–W1, in fact, could be explained, for example, by the random presence of field stars in the sample or by large photometric errors.

In the future we plan to use the lists of probable cluster members from Cantat-Gaudin et al. (2020) to investigate the binary and multiple star population of a larger number of clusters. Additionally, we will try to expand the range of stellar mass for the investigation.

The work of A.F.S. was supported by the Ministry of Science and Higher Education of the Russian Federation, FEUZ-2020-0030. The work of G.C. has been supported by Padova University grant BIRD191235/19: Internal dynamics of Galactic star clusters in the Gaia era: binaries, blue stragglers, and their effect in estimating dynamical masses.

ORCID iDs

Varvara O. Mikhnevich https://orcid.org/0000-0001-8514-3366
Giovanni Carraro https://orcid.org/0000-0002-0155-9434
Anton F. Seleznev https://orcid.org/0000-0001-8669-803X

References

Bardalez Gagliuffi, D. C., Burgasser, A. J., Gelino, C. R., et al. 2014, ApJ, 794, 143
Bonifazi, A., Fusi Pecci, F., Romeo, G., & Tosi, M. 1990, MNRAS, 245, 15

Borodina, O. I., & Kovaleva, D. A. 2020, INASAN Science Reports, 5, 351
Bressan, A., Marigo, P., Girardi, L., et al. 2012, MNRAS, 427, 127
Cantat-Gaudin, T., Anders, F., Castro-Ginard, A., et al. 2020, A&A, 640, A1
Cutri, R. M. & IPAC/WISE Science Data Center Team 2012, AAS Meeting Abstracts, 219, 401.06
Danilov, V. M., & Seleznev, A. F. 2020, AstBu, 75, 407
Dias, W. S., Monteiro, H., Moitinho, A., et al. 2021, MNRAS, 504, 356
Duchene, G., & Kraus, A. 2013, ARA&A, 51, 269
Duquennoy, A., & Mayor, M. 1991, A&A, 248, 485
El-Badry, K., Rix, H.-W., Tian, H., Duchene, G., & Moe, M. 2019, MNRAS, 489, 5822
Fisher, J., Schroder, K.-P., & Smith, R. C. 2005, MNRAS, 361, 495
Geißler, K., Metchev, S., Kirkpatrick, J. D., Berriman, G. B., & Looper, D. 2011, ApJ, 732, 56
Haffner, H., & Heckmann, O. 1937, VeGoe, 0004, 77
Khalaj, P., & Baumgardt, H. 2013, MNRAS, 434, 3236
Kouwenhoven, M. B. N., Brown, A. G. A., Goodwin, S. P., Portegies Zwart, S. F., & Kaper, L. 2009, A&A, 493, 979
Li, Z.-M., Mao, C.-Y., Luo, Q.-P., et al. 2017, RAA, 17, 071
Lodieu, N., Perez-Garrido, A., Smart, R. L., et al. 2019, A&A, 628, A66
Malkov, O., Mironov, A., & Sichevskij, S. 2010, EAS Publications Series, 45, 409
Malkov, O., Mironov, A., & Sichevskij, S. 2011, Ap&SS, 335, 105
Malofeeva, A. A., Seleznev, A. F., & Carraro, G. 2022, AJ, 163, 113
Maxted, P. F. L., Jeffries, R. D., Oliveira, J. M., Naylor, T., & Jackson, R. J. 2008, MNRAS, 385, 2210
Nikiforova, V. V., Kulesh, M. V., Seleznev, A. F., et al. 2020, AJ, 160, 142
Patience, J., Ghez, A. M., Reid, I. N., et al. 2002, AJ, 123, 1570
Raghavan, D., McAlister, H. A., Henry, T. J., et al. 2010, ApJS, 190, 1
Reggiani, M., & Meyer, M. R. 2013, A&A, 553, A124
Sarro, L. M., Bouy, H., Berihuete, A., et al. 2014, A&A, 563, A45
Sheikhi, N., Hasheminia, M., Khalaj, P., et al. 2016, MNRAS, 457, 1028
Skrutskie, M. F., Cutri, R. M., Stiening, R., et al. 2006, AJ, 131, 1163
Thompson, B. A., Frinchaboy, P. M., Spoo, T., et al. 2021, AJ, 161, 160